Talanta 107 (2013) 127–132

Contents lists available at SciVerse ScienceDirect

Talanta

journal homepage: www.elsevier.com/locate/talanta

A solid-state electrochemiluminescence sensing platform for detection of catechol based on novel luminescent composite nanofibers

Xiaoying Wang [a,*], Xiaobing Wang [b], Sumeng Gao [a], Yi zheng [a], Meng Tang [a], Baoan Chen [c]

[a] Key Laboratory of Environmental Medicine and Engineering, Ministry of Education, School of Public Health, Southeast University, Nanjing 210009, China
[b] Department of Natural Medicinal Chemistry, China Pharmaceutical University, Nanjing 210009, China
[c] Department of Hematology and Oncology (Key Department of Jiangsu Medicine), Zhongda Hospital, Medical School, Southeast University, Nanjing 210009, China

ARTICLE INFO

Article history:
Received 17 November 2012
Received in revised form
31 December 2012
Accepted 6 January 2013
Available online 11 January 2013

Keywords:
Luminescent composite nanofibers
Electrospinning
Solid-state electrochemiluminescence
$Ru(bpy)_3^{2+}$
Catechol

ABSTRACT

A solid-state electrochemiluminescence (ECL) sensing platform based on the novel luminescent composite nanofibers for detection of catechol has been developed. The carboxylated multi-walled carbon nanotubes (MWNTs) and ruthenium(II) tris-(bipyridine) ($Ru(bpy)_3^{2+}$) doped nylon 6 (PA6) luminescent composite nanofibers (Ru-MWNTs-PA6) were successfully fabricated by a one-step electrospinning technique. The Ru-MWNTs-PA6 nanofibers, with unique 3D nanostructure, large specific surface area and a larger amount of immobilized-$Ru(bpy)_3^{2+}$, maintained the photoelectric properties of the $Ru(bpy)_3^{2+}$ ions and exhibited excellent ECL behaviors on glassy carbon (GC) electrode. As a solid-state ECL sensing platform, the Ru-MWNTs-PA6 nanofibers can sensitively detect low concentration catechol by monitoring the phenol-dependent ECL intensity change. The detection limit for catechol is 1.0 nM, which is comparable or better than that in the reported assays. The solid-state ECL sensor displayed wide linear range, high sensitivity and good stability. It holds promise for the electrospun nanofibers-based ECL sensors have a great potential for routine analyses.

1. Introduction

Ruthenium(II) tris-(bipyridine) ($Ru(bpy)_3^{2+}$) is the most used electrochemiluminescence (ECL) substrate [1–3]. Solid-state $Ru(bpy)_3^{2+}$–ECL system can provide several advantages, such as supersensitive, cost-effective, the signal amplification, simplifying experimental design and creating a regenerable sensor based on $Ru(bpy)_3^{2+}$ recycled at the electrode surface during the ECL reaction [4–6]. It has become an important and valuable detection method in sensors. Until now, much effort has been made to immobilize $Ru(bpy)_3^{2+}$ on electrode surfaces by different techniques [5–7], such as Langmuir–Blodgett [8,9], selfassembled monolayers [10,11], layer-by-layer assembly [12], cation exchange polymers [13,14] and $Ru(bpy)_3^{2+}$-doped nanomaterials [15,16]. However, these approaches are time-consuming or involve complicated fabrication processes. It is widely accepted that the following aspects, the surface area of the sensing platform and the amount of immobilized $Ru(bpy)_3^{2+}$ on the electrode surface, will contribute to an increase of the solid-state ECL sensor's sensitivity [17]. So it is still desired to develop a new, facile, highly efficient and inexpensive approach for fabricating solid-state $Ru(bpy)_3^{2+}$–ECL sensor interfaces which have large surface area and high amount of immobilized $Ru(bpy)_3^{2+}$.

Electrospinning has been proved to be a simple, versatile and cost-effective approach to fabricate polymeric nanofibers [18,19]. Compared with conventional planar materials, the ultrafine nanofibers have several advantages of uniformity, porosity, mechanical strength, high surface area to volume ratio and multiple active sites for various further interaction or modifications [20,21]. Many studies have utilized electrospun nanofibers for biomedical and industrial applications, such as the supporting scaffolds for enzyme immobilization [22], the membranes for filtration [23], the tissue templates [24], the artificial organ implant and the drug delivery [25]. It is believed that electrospun nanofibers can be used as an ideal platform for highly sensitive sensing applications with all of the aforementioned advantages [26]. Several reports have investigated the development of nanofiber-based ECL sensing platforms for molecular detection, such as phenol [27], hydroquinone [28] and atropine [29]. But ECL sensing platform based on electrospun luminescent composite nanofibers has never been applied to detect the catechol.

Catechol, a kind of phenolic compounds, is widely used for synthesis in food, pharmaceuticals or agrochemical ingredients, but also as stabilizing additives [30–32]. Catechol and its derivatives are also found in biological systems, and play a significant role in many biochemical processes. For example, catecholamines are important neurotransmitters in the central nervous system. Abnormal levels of

* Corresponding author. Tel.: +86 25 83272563; fax: +86 25 83272561.
E-mail address: wxy@seu.edu.cn (X. Wang).

0039-9140/$ - see front matter © 2013 Elsevier B.V. All rights reserved.
http://dx.doi.org/10.1016/j.talanta.2013.01.007

catecholamines in the brain are linked to diseases such as Parkinson's, and changes in plasma concentrations of different catechol act as indicators for several diseases [33]. Therefore, sensitive and rapid detection of catechol is of great value.

Herein we provided another successful example to demonstrate that the electrospinning technique could be used to develop highly efficient solid-state ECL sensor. The carboxylated multi-walled carbon nanotubes (MWNTs) and Ruthenium(II) tris-(bipyridine) ($Ru(bpy)_3^{2+}$) doped nylon 6 (PA6) luminescent composite nanofibers (Ru-MWNTs-PA6) were successfully fabricated by a one-step electrospinning technique as shown in Fig. 1. The Ru-MWNTs-PA6 nanofibers exhibit some advantages over the common $Ru(bpy)_3^{2+}$ ECL system in terms of ease of fabrication, strong ECL intensity and sensitive response to catechol. The solid-state ECL sensing strategy based on the novel Ru-MWNTs-PA6 for detection of catechol has been designed. The characteristics of the sensing system for the detection of catechol and the analytical performance were evaluated.

2. Experiment section

2.1. Reagents and apparatus

$Ru(bpy)_3Cl_2 \cdot 6H_2O$ (99.95%), catechol and tri-*n*-propylamine (TPrA, 98%) were purchased from Sigma (USA). Nylon 6 (PA6) material was purchased from Debiochem (China). Carboxylated multi-walled carbon nanotubes (MWNTs) were obtained from Shenzhen Nanotech Port Co. Ltd. (China). The diameter was 40–60 nm and the length 1–10 μm. Other reagents were of analytical reagent grade. All the solutions were prepared with ultrapure water from a Millipore Milli-Q system.

The field-emission scanning electron microscope (FESEM) images were recorded using S-4800 FE-SEM (JEOL., Japan). The fluorescence photographs were recorded using IX71-F22FL/PH inverted fluorescence microscope (Olympus, Japan). ECL was measured with MPI-E electrochemiluminescence analyzer (Remax Electronic Science Tech. Co. Ltd., China), cyclic voltammogram (CV) was recorded with a CHI 660D electrochemical analyzer (CHI instruments Inc., Chenhua Corp., China).

2.2. Electrospinning

The electrospinning apparatus was similar to those described before [17]. A series of electrospinning solutions were prepared by dissolving PA6 and MWNTs in mixture of cresol and formic acid (6:4, V/V) at desired weight ratios. If added, the concentration of $Ru(bpy)_3^{2+}$ was 0.2 wt%. In order to obtain a homogeneous solution, the mixed solution was under vigorous stirring for 6 h at room temperature. Electrospinning was carried out with a 20 mL syringe (1.2 mm diameter spinneret) at electrical potential of 15 kV over a 15 cm gap between the spinneret and the aluminium sheet with a rate of 1.0 mL h^{-1}. The ambient temperature and relative humidity for electrospinning were kept at 25 °C and 40%, respectively. It took 3 min to deposit the nanofibers on the surface of the aluminium sheet acceptor. After the electrospun fibrous membrane was formed, it was gently striped from the aluminium sheet acceptor, placed over a beaker, and dried in an oven at 140 °C for 20 min.

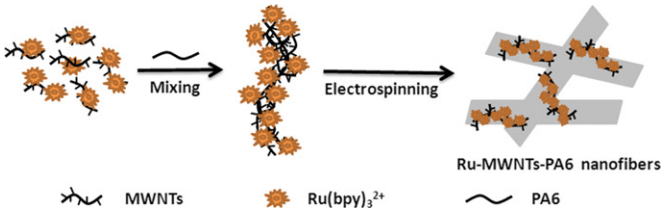

Fig. 1. Schematic representation of the one-step process for fabricating the Ru-MWNTs-PA6 luminescent composite nanofibers.

2.3. Preparation of the working electrode

The surface of glassy carbon (GC) electrode was carefully polished with 0.3 μm Al_2O_3 powders successively, rinsed with water and ethanol in an ultrasonic bath briefly and then allowed to dry at room temperature. Two different $Ru(bpy)_3^{2+}$-modified electrodes were prepared as following: (1) The Ru-MWNTs-PA6 film electrode. A clean GC electrode surface was coated with 2.0 μL electrospinning solution (containing $Ru(bpy)_3^{2+}$ (0.2 wt%), PA6 (31 wt%) and MWNTs (0.8 wt%)), and then dried at room temperature; The as-prepared electrode was denoted as the Ru-MWNTs-PA6 film electrode. (2) The Ru-MWNTs-PA6 nanofibers electrode. It took 3 min to deposit the nanofibers on the surface of a clean GC electrode by electrospinning the same solution to (1). The as-prepared electrode was denoted as the Ru-MWNTs-PA6 nanofibers electrode.

2.4. Measurement

The ECL determinations were performed at room temperature in a 10 mL homemade quartz cell. A three-electrode system was used with the modified GC electrode (3 mm in diameter) as the working electrode, an Ag/AgCl (sat.) as the reference electrode and a platinum wire as the counter electrode. Cyclic voltammetry mode with continuous potential scanning from 0.0 to 1.2 V and scanning rate of 100 mV s^{-1} was applied to achieve ECL signal in 20 mM phosphate buffer solution (PBS) containing 1.0 mM TPrA (pH 8.0). A high voltage of −800 V was supplied to the photomultiplier for luminescence intensity determination. The ECL and CV curves were recorded simultaneously.

3. Results and discussion

3.1. FESEM image of the Ru-MWNTs-PA6 luminescent composite nanofibers

The micro-morphologies of the Ru-MWNTs-PA6 luminescent composite nanofibers were analyzed using FESEM as shown in Fig. 2. The Ru-MWNTs-PA6 composite nanofibers with smooth surface, evenly distributed on the substrate with their random orientations, form a porous 3D structure nanofibrous membrane (Fig. 2A). The diameters of the Ru-MWNTs-PA6 nanofibers range from 50 to 500 nm (Fig. 2B). More uniform diameter fibers may be achieved by changing the conditions of the electrospinning process. The electrospinning related parameters including PA6 concentration, applied voltage, collector distance, feed rate etc., and their individual and interactive effects on the diameter of the Ru-MWNTs-PA6 luminescent composite nanofibers were experimentally investigated. The fiber diameter was detected to be more responsive to PA6 concentration than to voltage and distance in the experiment range. The ratio of voltage to distance and the ratio of PA6 concentration to distance were found to be important in predicting the trend of fiber diameter. Applied voltage was come to be an insignificant factor when PA6 concentration and collector distance were high. The collector distance may be increased in favor of reducing the fiber diameter. The above results are consistent with the report in the literature [34,35].

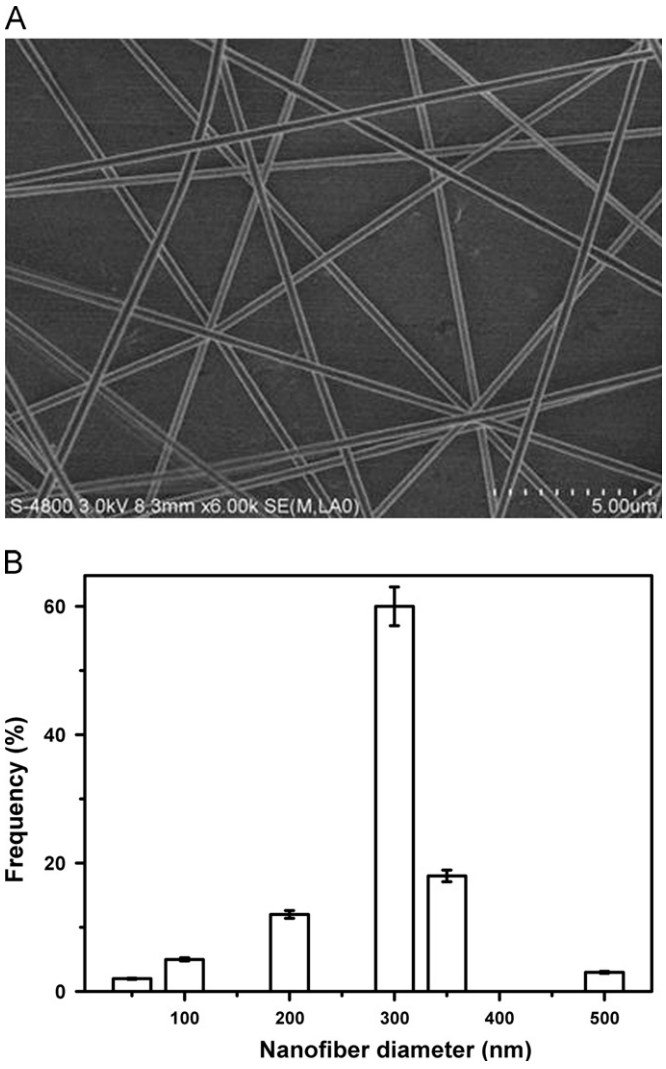

Fig. 2. (A) FESEM image of the Ru-MWNTs-PA6 luminescent composite nanofibers. PA6 (31 wt%), MWNTs (0.8 wt%), $Ru(bpy)_3^{2+}$ (0.2 wt%), 7 spinneret, 15 cm gap, 0.8 mL h^{-1} rate, 15.1 kV electrical potential, the diameters of the nanofibers was 300 nm. (B) The diameter distribution of the Ru-MWNTs-PA6 luminescent composite nanofibers.

3.2. Fluorescence photographs of the Ru-MWNTs-PA6 luminescent composite nanofibers

The fluorescence photographs of the Ru-MWNTs-PA6 luminescent composite nanofibers ($Ru(bpy)_3^{2+}$ (0.2 wt%), PA6 (31 wt%) and MWNTs (0.8 wt%)) were recorded using inverted fluorescence microscope as shown in Fig. 3. The fluorescence photographs show that the Ru-MWNTs-PA6 luminescent composite nanofibers emit bright orange light at 610 nm and the luminosities are uniform when the photographs magnified at 400 times. The results are in agreement with the characteristics of free $Ru(bpy)_3^{2+}$ ion, which convinces that the Ru-MWNTs-PA6 luminescent composite nanofibers with a porous 3D structure properly maintain the luminescent property of $Ru(bpy)_3^{2+}$ ions. Furthermore, the existence of the polymer hybrid matrixes can improve the thermal and optical stability of the $Ru(bpy)_3^{2+}$ complex and elongate the fluorescence lifetime of the $Ru(bpy)_3^{2+}$ complex. Due to the outstanding fluorescent property, the Ru-MWNTs-PA6 luminescent composite nanofibers show potential applications in sensors and preparation of various polymer optoelectronic micro/nano materials.

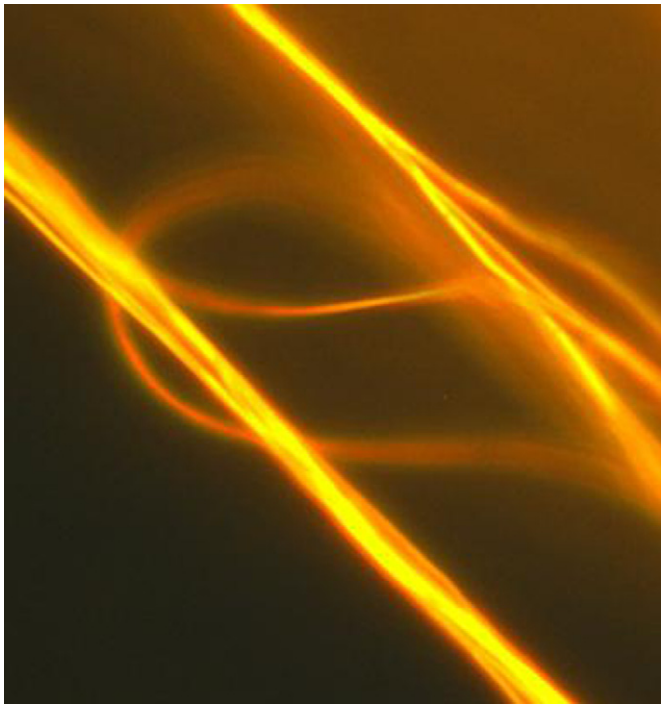

Fig. 3. Fluorescence photograph of the Ru-MWNTs-PA6 luminescent composite nanofibers magnified at 400 times.

3.3. The characterization of the Ru-MWNTs-PA6 luminescent composite nanofibers

The electrochemical surface area has been evaluated according to the reported protocols [16]. Compared with the bare GC electrode, the electrochemical surface area of the Ru-MWNTs-PA6 nanofibers electrode increased from 0.071 to 0.229 cm^2. It was resulted from the fact that numerous Ru-MWNTs-PA6 nanofibers existed on the GC electrode surface, of which each Ru-MWNTs-PA6 nanofiber having a large surface area can be regarded as an independent micro electrode when the electrochemical reaction taken place on the Ru-MWNTs-PA6 nanofibers electrode. By this way, a significantly increasing of the oxidation current around Ru-MWNTs-PA6 nanofibers was achieved. Finally, the Ru-MWNTs-PA6 nanofibers with 3D porous structure produced by electrospinning can increase the electrochemical surface area effectively.

The ECL intensity-potential curve of the Ru-MWNTs-PA6 nanofibers electrode in 20 mM PBS containing 1 mM TPrA (pH 8.0) is shown in Fig. 4. The ECL signal increases sharply at 0.9 V and reaches its peak at 1.17 V, which is almost the same as that of free $Ru(bpy)_3^{2+}$ under the same experimental conditions. The ECL signal of the Ru-MWNTs-PA6 nanofibers electrode in the presence of 1.0 mM TPrA (Fig. 4A, curve a) was stronger than that obtained without TPrA (Fig. 4A, curve b), and the Ru-MWNTs-PA6 luminescent composite nanofibers had a pair of obvious redox peaks of $Ru(bpy)_3^{2+}$ at CV curve (Fig. 4B). These results are in agreement with the characteristics of free $Ru(bpy)_3^{2+}$ ion [36,37], which convinces that the Ru-MWNTs-PA6 luminescent composite nanofibers with a porous 3D structure properly maintain the electrical properties of the $Ru(bpy)_3^{2+}$ ions.

In order to demonstrate the advantage of the Ru-MWNTs-PA6 luminescent composite nanofibers in ECL amplification, we compared the different ECL behaviors between a thin film, and Ru-MWNTs-PA6 nanofibers on GC electrode (for fabrication details, see the experimental section), respectively. As shown in Fig. 5, for the Ru-MWNTs-PA6 nanofibers electrode, the ECL peak reached 1.17 V and the ECL intensity was 953 a.u. The ECL intensity almost unchanged in 20 mM

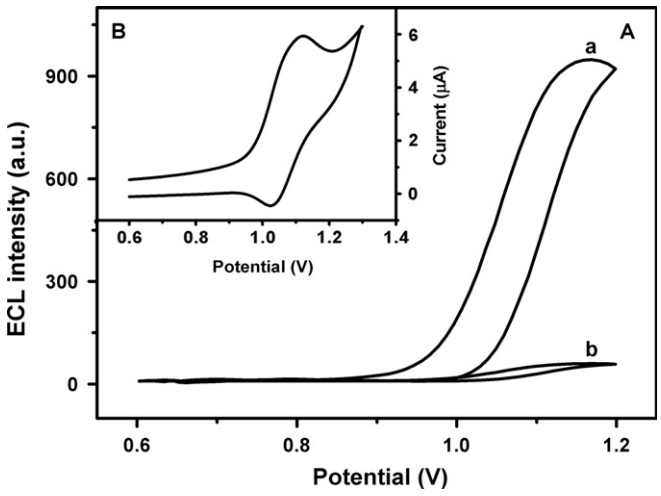

Fig. 4. (A) The ECL intensity of the Ru-MWNTs-PA6 nanofibers electrode in present (a) and absent (b) of 1.0 mM TPrA–20 mM PBS (pH 8.0). (B) The cyclic voltammogram of the Ru-MWNTs-PA6 nanofibers electrode in 20 mM PBS (pH 8.0). Scan rate: 100 mV s^{-1}, scan range: 0.6–1.4 V.

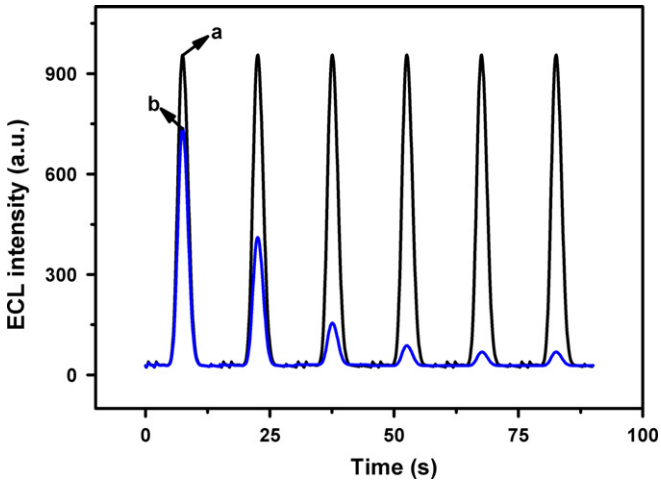

Fig. 5. The ECL curves of the Ru-MWNTs-PA6 nanofibers electrode and the Ru-MWNTs-PA6 film electrode in 20 mM PBS containing 1.0 mM TPrA (pH 8.0), under continuous CVs for 6 cycles. Scan rate: 100 mV s^{-1}, scan range: 0.6–1.2 V. (a) the Ru-MWNTs-PA6 nanofibers electrode, (b) the Ru-MWNTs-PA6 film electrode.

PBS containing 1.0 mM TPrA (pH 8.0) during continuous CV scans for 6 cycles (curve a). Thus, electronspun nanofibers can be used as the attractive host matrix for the available loading of guest molecules ($Ru(bpy)_3^{2+}$) in the electrode modification. The ECL intensity of the Ru-MWNTs-PA6 film electrode was 736 a.u. in 20 mM PBS containing 1.0 mM TPrA (pH 8.0) under the first CV cycle (curve b). However, the ECL intensity of the Ru-MWNTs-PA6 film electrode was becoming smaller and smaller during continuous CV scans for 6 cycles, at last, the ECL intensity was only 67 a.u. (curve b). Since the thin film and the Ru-MWNTs-PA6 nanofibers are both fabricated with the same electrospinning solution, the ECL intensity of the Ru-MWNTs-PA6 nanofibers is about 14.2 times higher than that of the thin film after continuous CV scans for 6 cycles as shown in Fig. 5. It might be attributed to the high surface area to volume ratio, and the uniform, stable and efficient immobilization of $Ru(bpy)_3^{2+}$. TPrA, a small molecule, acted as an ECL coreactant, can penetrate freely into the Ru-MWNTs-PA6 nanofibers matrix and react with the immobilized guest molecules ($Ru(bpy)_3^{2+}$). As a result, an enhanced response presented due to the porous structure of the electrospun nanofibers. Moreover, the outstanding charge-transport characteristics of the MWNTs might greatly promote the electron-transfer reactions of the Ru-MWNTs-PA6 nanofibers electrode surface. Finally, the Ru-MWNTs-PA6 nanofibers exhibited excellent ECL behaviors on GC electrode.

The ECL intensity of the Ru-MWNTs-PA6 nanofibers electrode almost unchanged during continuous CV scans for 30 cycles. It indicates a good stability of the ECL signal of the electrospun nanofibers. The Ru-MWNTs-PA6 nanofibers electrode was immersed in 20 mM PBS containing 1.0 mM TPrA (pH 8.0) for 10 h, and no ECL signal was detected for the above PBS. It is attributed to the fact that negatively charged COOH-MWNTs, with a high specific surface area, immobilized stably a large number of positively charged $Ru(bpy)_3^{2+}$ in the form of composites via electrostatic interaction in the porous 3D structure nanofibrous membrane, and a trace amount of MWCNTs could increase the mechanical stability of nanofibers, and make them more durable under operating conditions.

3.4. Optimization of experimental conditions

In order to maximize the detection sensitivity of the proposed solid-state ECL sensor, various conditions were optimized by single factor experiments. The depositing time of the Ru-MWNTs-PA6 nanofibers on the surface of the GC electrode was investigated. In 3 min, the Ru-MWNTs-PA6 nanofibers were deposit on the surface of the GC electrode, and were visible directly. So, we employed 3 min to deposit the Ru-MWNTs-PA6 nanofibers on the surface of the GC electrode by electrospinning the solution (containing $Ru(bpy)_3^{2+}$ (0.2 wt%), PA6 (31 wt%) and MWNTs (0.8 wt%)). In such conditions, Ru-MWNTs-PA6 nanofibers electrode has not only the outstanding charge-transport characteristics but also the good stability.

In order to examine the effect of doped concentration of $Ru(bpy)_3^{2+}$ on the luminescent intensity, four different amounts of $Ru(bpy)_3^{2+}$ (0.1, 0.15, 0.2, 0.3 wt%) were doped to the nanofibers. It is obvious that the luminescent intensity increases with the increment of doping concentration, and reaches the maximum at the doping concentration of 0.2 wt%. The luminescent intensity decreases at 0.3 wt%. It indicates that the concentration quenching may dominate when the concentration is higher than 0.2 wt%. In other words, when the concentration is higher than 0.2 wt%, the strong self-quenching and triplet–triplet annihilation between ruthenium(II) complex in the composite fibers may decrease the emission efficiency.

The determination buffer solution has great impact on ECL intensity. The concentration effects of TPrA and the pH of the PBS on the ECL intensity of the Ru-MWNTs-PA6 nanofibers electrode were investigated. The curve that the ECL intensity varied with the concentration of the TPrA from 0 to 2.0 mM with an increment of 0.5 mM was like a parabola and its peak was at 1.0 mM. So, 1.0 mM was chosen as the concentration of the TPrA. The ECL intensity increased greatly with the pH value increasing until it reached a plateau in the pH 7.5–8.5 and declined sharply at the pH > 8.5. So, 8.0 was chosen as the pH value of the PBS at the following experiment.

3.5. The analytical performance of the solid-state ECL sensing platform

Phenolic compounds are pharmaceutically and environmentally important compounds. It has been reported that phenolic compounds exhibit a quenching effect on $Ru(bpy)_3^{2+}$ ECL signals due to the energy transfer from the excited state $Ru(bpy)_3^{2+*}$ to the electro-oxidation species of phenolic compounds [38,39]. In this work, different quenching efficiencies between catechol, hydroquinone, resorcin, benzoquinone and phenol were observed. The quenching efficiency is defined as $(I_{ECL}^0 - I_{ECL})/I_{ECL}^0$, where I_{ECL} and I_{ECL}^0 represent the ECL intensity with and without the quencher, respectively. As shown in Table 1, catechol and resorcin show high quenching efficiencies. With a concentration of 200 μM, they display quenching

Table 1
The quenching efficiencies of the phenolic compounds in 20 mM PBS containing 1.0 mM TPrA and 200 μM phenolic compound (pH 8.0).

Compound[a]	Catechol	Hydroquinone	Resorcin	Benzoquinone	Phenol
$(I_0-I)/I_0$ (%)	68.5	61.7	70.1	67.6	53.9

[a] The concentration of the compound is 200 μM, the fluctuation range of the quenching efficiency is ±5%. Scan rate: 100 mV s^{-1}, scan range: 0.0–1.2 V.

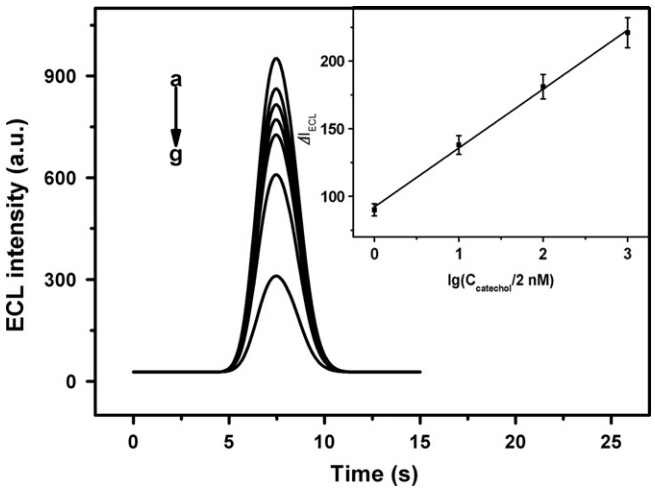

Fig. 6. The ECL response of the Ru-MWNTs-PA6 nanofibers electrodes in 20 mM PBS containing various concentrations of catechol. The concentrations of catechol were 0 M (a), 2 nM (b), 20 nM (c), 200 nM (d), 2 μM (e), 20 μM (f) and 200 μM (g), respectively. Inset: the calibration curves of catechol detection. The concentrations of catechol were 2 nM, 20 nM, 200 nM and 2 μM, respectively. ECL signals were achieved in 20 mM PBS containing 1.0 mM APrA (pH 8.0). Scan rate: 100 mV s^{-1}, scan range: 0.0–1.2 V.

efficiencies of 68.5% and 70.1%, respectively. Although phenol can hardly match the quenching efficiencies above at the same concentration, they also exhibit efficiently quenching efficiencies of 53.9%. This offers great potential for detecting phenolic compounds using Ru-MWNTs-PA6 nanofibers-based solid-state ECL sensing platform. However, the separation steps could be needed when the ECL sensing platform applied in the phenolic real samples.

The relative standard deviation (RSD) of the ECL intensity for the seven repeated detections of catechol (200 μM) was 4.83%, indicating the good reproducibility of this method. The stability of the Ru-MWNTs-PA6 nanofibers electrode was investigated after 10 days storage at room temperature and further used to incubate with the catechol, 96.1% of the initial sensitivity remained, suggested this modified electrode was a stable sensing platform. So, the solid-state ECL catechol sensor displayed good performance including long shelf life and excellent reproducibility.

Moreover, after the catechol test, the solid-state ECL sensing platform can be regenerated by immersing it into the ultrapure water, and rinsing it for several times to remove the adsorbed catechol and TPrA thoroughly. After the treatments, the platform is ready to incubate with the catechol again and for next catechol detection. Under the identical conditions, the platform can be continuously reused for 10 times, while still keeping the ECL response to 91.3% of its original state. As 90% of the original signal response is generally acceptable, our results indicate that this platform can be reused at least for 10 times repeatedly.

3.6. The calibration curve of catechol detection

The sensitivity of the solid-state ECL sensor was investigated. ECL responses of the Ru-MWNTs-PA6 nanofibers electrodes in 20 mM PBS containing various concentrations of catechol are shown in Fig. 6. The ECL intensity difference [ΔI_{ECL}, $\Delta I_{ECL}=I^0_{ECL}$(the ECL intensities without catechol)$-I_{ECL}$(the ECL intensities with catechol)] of the Ru-MWNTs-PA6 nanofibers electrodes grew when the catechol concentration increased, and the ΔI_{ECL} was found to be linear with the logarithm of catechol concentration in the range from 2 nM to 2 μM (as shown in the inset). The equation for the resulting calibration plot was $y=43.6\lg x+92.1$ (x was the concentration of catechol divide 2 nM, y was the ΔI_{ECL}), the correlation coefficient was 0.9991, and a detection limit of 1.0 nM was estimated by using 3σ (where σ is the relative standard deviation of a blank solution, $n=11$). The consistent data was obtained as shown in the error bar in the inset of the Fig. 6 when the experiment was repeated three times.

4. Conclusions

In this paper, a new, simple and general solid-state ECL sensing platform for detection of catechol has been designed. The luminescent composite nanofibers Ru-MWNTs-PA6 were successfully fabricated by a one-step electrospinning technique. As a sensing platform, the Ru-MWNTs-PA6 nanofibers with unique 3D nanostructure, large specific surface area and good stability exhibited excellent ECL behaviors on GC electrodes. A high quenching efficiency on the ECL signal was obtained with the presence of low concentration catechol compounds. The solid-state ECL sensor displayed wide linear range, high sensitivity and good stability. The assay allows detection at levels as low as 1.0 nM of the catechol. The results demonstrate that electrospinning technique can be used to develop highly efficient solid-state ECL sensors. Moreover, the strategy could be extended to develop various solid-state ECL sensors for the detection and quantification of many kinds of analytes, such as phenol, benzoquinone, other phenolic compounds, etc.

Acknowledgment

Project supported by the National Key Basic Research Program 973 (No. 2010CB732404), the National Important Project on Scientific Research of China (No. 2011CB933404), the National Nature Science Foundation of China (Nos. 30972504, 81172697 and 81170492), the Doctoral Program of Higher Education of China (No. 20110092120055), the Key Department of Jiangsu Medicine (No. 2012-12), the Innovation Fund of Southeast University (No. 3225000501) and the Open Research Fund of State Key Laboratory of Bioelectronics of Southeast University.

References

[1] M.M. Richter, Chem. Rev. 104 (2004) 3003–3036.
[2] W.J. Miao, A.J. Bard, Anal. Chem. 76 (2004) 5379–5386.
[3] W. Zhan, A.J. Bard, Anal. Chem. 79 (2007) 459–463.
[4] W.J. Miao, Chem. Rev. 108 (2008) 2506–2553.
[5] H. Wei, E.K. Wang, Trends Anal. Chem. 27 (2008) 447–459.
[6] M. Su, S.Q. Liu, Anal. Biochem. 402 (2010) 1–12.
[7] P. Bertoncello, R.J. Forster, Biosens. Bioelectron. 24 (2009) 3191–3200.
[8] X. Zhang, A.J. Bard, J. Am. Chem. Soc. 111 (1989) 8098–8105.
[9] C.H. Lyons, E.D. Abbas, J.K. Lee, M.F. Rubner, J. Am. Chem. Soc. 120 (1998) 12100–12107.
[10] Z. Zhang, A.J. Bard, J. Phys. Chem. 92 (1988) 5566–5569.
[11] X.P. Sun, Y. Du, L.X. Zhang, S.J. Dong, E.K. Wang, Anal. Chem. 79 (2007) 2588–2592.
[12] Z.H. Guo, Y. Shen, M.K. Wang, F. Zhao, S.J. Dong, Anal. Chem. 76 (2004) 184–191.
[13] S.N. Ding, J.J. Xu, H.Y. Chen, Electrophoresis 26 (2005) 1737–1744.
[14] Y.F. Zhuang, D.M. Zhang, H.X. Ju, Analyst 130 (2005) 534–540.
[15] W. Gao, X.H. Xia, J.J. Xu, H.Y. Chen, J. Phys. Chem. C 111 (2007) 12213–12219.

[16] X.Y Wang, X.Y. Zhang, P.G. He, Y.Z. Fang, Biosens. Bioelectron. 26 (2011) 3608–3613.
[17] D. Shan, B. Qian, S.N. Ding, W. Zhu, S. Cosnier, H.G. Xue, Anal. Chem. 82 (2010) 5892–5896.
[18] N. Bhardwaj, S.C. Kundu, Biotechnol. Adv. 28 (2010) 325–347.
[19] S. Chigome, N. Torto, Anal. Chim. Acta 706 (2011) 25–36.
[20] Z.G. Wang, L.S. Wan, Z.M. Liu, X.J. Huang, Z.K. Xu, J. Mol. Catal. B: Enzym. 56 (2009) 189–195.
[21] S.H. Jiang, H.Q. Hou, A. Greiner, S. Agarwal, Appl. Mater. Interfaces 4 (2012) 2597–2603.
[22] S. Huang, Y. Ding, Y.X. Liu, L. Su, R. Filosa Jr, Y. Lei, Electroanalysis 23 (2011) 1912–1920.
[23] Q. Xu, N.P. Zhang, X.Y. Yin, M. Wang, Y.Y. Shen, S. Xu, L. Zhang, Z.Z. Gu, J. Chromatogr. B 878 (2010) 2403–2408.
[24] M. Maas, P. Guo, M. Keeney, F. Yang, T.M. Hsu, G.G. Fuller, C.R. Martin, R.N. Zare, Nano Lett. 11 (2011) 1383–1388.
[25] N. Naveen, R. Kumar, S. Balaji, T.S. Uma, T.S. Natrajan, P.K. Sehgal, Adv. Eng. Mater. 12 (2010) B380–B387.
[26] S. Marx, M.V. Jose, J.D. Andersen, A.J. Russell, Biosens. Bioelectron. 26 (2011) 2981–2986.
[27] C.S. Zhou, Z. Liu, J.Y. Dai, D. Xiao, Analyst 135 (2010) 1004–1009.
[28] Z. Liu, C.S. Zhou, B.Z. Zheng, L. Qian, Y. Mo, F.L. Luo, Y.L. Shi, M.M.F. Choi, D. Xiao, Analyst 136 (2011) 4545–4551.
[29] X.Y. Yang, C.Y. Xu, B.Q. Yuan, T.Y. You, Chin. J. Anal. Chem. 39 (2011) 1233–1237.
[30] M.C.J. Dekker, V. Bonifati, C.M. Van Duijn, Brain 126 (2003) 1722–1733.
[31] M. Some, A. Helander, Life Sci. 71 (2002) 2341–2349.
[32] B. Wolfrum, M. Zevenbergen, S. Lemay, Anal. Chem. 80 (2008) 972–977.
[33] Y.B. Wu, J.H. Wu, Z.G. Shi, Y.Q. Feng, J. Chromatogr. B 877 (2009) 1847–1855.
[34] O.S. Yördem, M. Papila, Y.Z. Menceloğlu, Mater. Des. 29 (2008) 34–44.
[35] L.Y. Kong, G.R. Ziegler, Carbohydr. Polym. 92 (2013) 1416–1422.
[36] J.K. Leland, M.J. Powell, J. Electrochem. Soc. 137 (1990) 3127–3131.
[37] W.J. Miao, J.P. Choi, A.J. Bard, J. Am. Chem. Soc. 124 (2002) 14478–14485.
[38] H.Z. Zheng, Y.B. Zu, J. Phys. Chem. B 109 (2005) 16047–16051.
[39] J. McCall, C. Alexander, M.M. Richter, Anal. Chem. 7 (1999) 2523–2527.